Main Manuscript for

Proximity interactome analysis of Lassa polymerase reveals eRF3a/GSPT1 as a druggable target for host directed antivirals.

Jingru Fang[1,2], Colette Pietzsch[3,4], George Tsaprailis[5], Gogce Crynen[5], Kelvin Frank Cho[6], Alice Y. Ting[7,8,] Alexander Bukreyev[3,4,9], Erica Ollmann Saphire[2]* and Juan Carlos de la Torre[1]*

[1] Department of Immunology and Microbiology, Scripps Research, La Jolla CA 92037

[2]La Jolla Institute for Immunology, La Jolla CA 92037

[3]Department of Pathology, University of Texas Medical Branch, Galveston, TX 77550

[4]Galveston National Laboratory, University of Texas Medical Branch, Galveston, TX 77550

[5]Proteomics Core, Scripps Research, Jupiter, FL 33458

[6]Cancer Biology Program, Stanford University, Stanford, CA 94305

[7]Department of Genetics, Department of Biology and Department of Chemistry, Stanford University, Stanford, CA 94305

[8]Chan Zuckerberg Biohub, San Francisco, CA 94158

[9]Department of Microbiology and Immunology, University of Texas Medical Branch, Galveston, TX 77550

*Erica Ollmann Saphire; Juan Carlos de la Torre.

Email: erica@lji.org and juanct@scripps.edu

Author Contributions: J.F., E.O.S., and J.C.T designed research; J.F. performed all non-BSL4 experiments and analyzed data; C.P. performed all BSL-4 experiments; A.B. provided supervision to BSL4 research; G.T. and G.C performed proteomic experiments and analyses; K.F.C. and A.Y.T provided a critical resource; J.F., E.O.S., and J.C.T wrote the paper. All authors reviewed and edited the paper.

Competing Interest Statement: The authors declare no competing interest.

Classification: Biological Sciences (Microbiology; Biochemistry)

Keywords: Viral replication, Proximity proteomics, Host-virus interactions

This PDF file includes:

Main Text
Figures 1 to 6

Abstract

Completion of the Lassa virus (LASV) life cycle critically depends on the activities of the virally encoded RNA-dependent RNA polymerase in replication and transcription of the negative-sense RNA viral genome in the cytoplasm of infected cells. We hypothesized that interactions with an array of cellular proteins may enable LASV polymerase to execute distinct viral RNA biosynthetic processes. To investigate this hypothesis, we applied proximity proteomics to define the interactome of LASV polymerase in cells, under conditions that recreate viral transcription and replication. We engineered a LASV polymerase-biotin ligase TurboID fusion protein that retained polymerase activity and successfully biotinylated the proximal proteome, which allowed us to identify 42 high-confidence hits that interact with LASV polymerase. We performed an siRNA screen to evaluate the role of the identified interactors in LASV infection, which uncovered six host factors for which their depletion affected LASV infection. We found that one polymerase interactor, eukaryotic peptide chain release factor subunit 3a (eRF3a/GSPT1), physically and functionally associated with LASV polymerase, exhibiting proviral activity. Accordingly, pharmacological targeting of GSPT1 resulted in strong inhibition of LASV infection. In summary, our work demonstrates the feasibility of using proximity proteomics to illuminate and characterize yet to be defined, host-pathogen interactomes, which can reveal new biology and uncover novel targets for the development of antivirals against LASV.

Significance Statement

Lassa virus (LASV), the causative agent of Lassa fever (LF), poses an important public health problem in Western Africa, and current therapeutic interventions are very limited. Due to its limited genome coding capacity, LASV proteins are often multifunctional and orchestrate complex interactions with cellular factors to execute the steps required to complete its viral life cycle. LASV polymerase is essential for the replication and expression of the viral genome, and it is consequently an attractive target for antiviral intervention. Here we present the first host interactome of LASV polymerase, which can guide the identification of novel druggable host cellular targets for the development of cost-effective antiviral therapies against LF.

Main Text

Introduction

Lassa virus (LASV) is a mammarenavirus highly prevalent in Western Africa, where it infects several hundred thousand individuals annually, resulting in a substantial number of Lassa fever (LF) disease cases, associated with high morbidity and significant mortality with high case-fatality rates (CFRs) among hospitalized LF patients (WHO). While rodent-to-human transmission is the main contributor to human LASV infection, a significant number of LF cases can arise from human-to-human transmission (1). Moreover, LASV expansion outside its traditional endemic areas and increased travel have resulted in exported LF cases from endemic Western African countries to non-endemic countries (2). To date, no US Food and Drug Administration (FDA) licensed countermeasures are available to prevent or treat LASV infections, and current anti-LASV therapy is limited to an off-label use of ribavirin that has limited efficacy and can cause significant side effects. Hence, there is an unmet need for therapeutics to combat LASV infections, a task that would be facilitated by a better understanding of virus-host cell interactions that modulate replication and gene expression of LASV in infected cells.

Like other mammarenaviruses (*Bunyavirales: Arenaviridae*), LASV is an enveloped virus with a bi-segmented, single-stranded RNA genome. Each viral genome segment uses an ambisense coding strategy to direct the synthesis of two viral proteins from open reading frames separated by non-coding intergenic regions (IGRs). The small (S) segment encodes the nucleoprotein (NP), which is responsible for genome encapsidation and immune evasion, and the glycoprotein precursor (GPC), which is co- and post-translationally processed to generate the mature GP that

83 mediates virion cell entry via receptor-mediated endocytosis (3). The large (L) segment encodes
84 the large (L) protein, which functions as a viral RNA-directed RNA polymerase (RdRp), and the
85 matrix Z protein. NP encapsidates the viral genome and antigenome RNA species to form the viral
86 nucleocapsid (NC) to which L associates to form the two viral ribonucleoprotein complexes (vRNPs)
87 (of L and S segments). The resulting vRNP is responsible for directing replication and transcription
88 of the viral RNA genome. Cellular polymerases and translation machinery can neither read nor
89 translate the viral RNA genome. Instead, the LASV polymerase initiates viral transcription from the
90 genome promoter located at the 3' end of the viral genome, which is primed by a small fragment of
91 host-cell-derived, capped RNA fragment via a mechanism called cap-snatching. Primary
92 transcription results in synthesis of NP and L mRNAs from the S and L segments, respectively.
93 Subsequently, the virus polymerase adopts a replicase mode and moves across the intergenic
94 region (IGR) to generate a copy of the full-length antigenome RNA (cRNA). This cRNA serves as
95 a template for the synthesis of the GPC and Z mRNAs from the S and L segments, respectively,
96 as well as a template for the amplification of the corresponding genome vRNA species (4, 5).
97 Coordination of multiple domains with distinct enzymatic functions through conformational
98 rearrangement and the engagement of vRNA promoter elements with LASV polymerase have been
99 proposed to mediate the functional transitioning of LASV polymerase between a replicase and
100 transcriptase (6). In the present paper, we have investigated the possibility that host cell factors
101 can critically contribute to the distinct steps of viral RNA synthesis driven by LASV polymerase. As
102 a first and necessary step, we applied the recently developed proximity labeling technology to
103 characterize the cellular interactomes of LASV L polymerase in the context of viral RNA synthesis
104 in living cells. For the first time, we generated a functional LASV polymerase fusion to the
105 engineered promiscuous biotin ligase TurboID, which retains its polymerase activity and can
106 biotinylate its cellular interactors *in situ*. This approach allowed us to affinity-capture biotinylated
107 interactors, leading to the discovery of 42 high-confidence candidate interactors of the LASV
108 polymerase. We implemented a high-content imaging-based, siRNA screen using infection with
109 live LASV in the human hepatocyte Huh7 cell line, which identified six host factors that functionally
110 contributed to LASV infection. We further characterized one of these factors, eukaryotic peptide
111 chain release factor subunit 3a (eRF3a/GSPT1), and determined that it physically interacts with
112 LASV polymerase and is required for LASV infection. Accordingly, pharmacological targeting of
113 GSPT1 strongly inhibits LASV infection. Our results have improved our understanding of the
114 cellular proteins and pathways involved in LASV multiplication and illuminate novel therapeutic
115 strategies against a highly lethal human pathogen.
116
117 **Results**

118 **Generating a PL enzyme-LASV L fusion protein with polymerase and proximity labeling**
119 **activities.** We selected TurboID, an engineered promiscuous biotin ligase, for proximity labeling
120 due to its optimized labeling efficiency. TurboID labels exposed lysine residues on neighboring
121 proteins within a ~10 nm radius and is highly active, requiring <10 minutes of labeling time for
122 detectable activity (7). We incorporated TurboID together with an HA tag into the LASV L protein
123 at a site previously shown to tolerate incorporation of epitope tags without severely affecting
124 polymerase activity (8) (**Figure 1A**).
125 We confirmed that the LASV polymerase-TurboID fusion protein was functionally active using
126 a LASV minigenome (MG) system (**Figure S1**). This cell-based viral MG system recapitulates
127 LASV RNA synthesis using an intracellular reconstituted vRNP expressing a reporter gene of
128 interest, in this case, a fluorescent protein ZsGreen. The expression level of the minigenome-
129 encoded reporter serves as a surrogate measure of vRNP activity and as a comprehensive
130 measurement of LASV MG replication, transcription, and translation of the minigenome reporter
131 transcript (9).
132 We used a wild-type LASV L (L-WT) and an N-terminal HA tagged L (L-HA) as controls for
133 comparison with LASV L-TurboID in the context of measuring polymerase activity and protein
134 expression levels. Results from the LASV MG assay revealed that LASV L-TurboID fusion
135 polymerase (L-TurboID) retains 70% of WT activity, with slightly lower expression levels compared

136 to that of the L-HA control (**Figure 1B**). We validated the construct's proximity labeling activity by
137 detecting biotinylated proteins in cells expressing the viral polymerase-TurboID fusion together with
138 vRNP components. We found that LASV L-TurboID produced a broad range of biotinylated proteins
139 in the presence of exogenous biotin, and promiscuous labeling was observed in a time-dependent
140 manner (**Figure 1C**).
141 Because western blot analysis using soluble cell lysates does not illuminate the subcellular
142 localization of the biotinylated proteins, we used confocal fluorescent microscopy to detect in-cell
143 biotinylation by LASV L-TurboID in fixed cell specimens. For these studies, we transfected
144 HEK293T cells with LASV MG system components, either with LASV L-TurboID or L-HA control,
145 followed by one-hour of biotin labeling, 24 hours post-transfection. We observed that LASV L-
146 TurboID localized to discrete puncta connecting patches in the cytoplasm, similar to the N-terminal
147 HA-tagged L control (L-HA). Furthermore, the biotinylation signal overlapped with the location of L-
148 TurboID, suggesting efficient and localized biotinylation mediated by the LASV L-TurboID (**Figure**
149 **1D)**.

150 **Defining LASV polymerase interactomes by proximity proteomics.** To set up the proximity
151 labeling-based proteomics experiment, we transfected HEK 293T cells with LASV MG system
152 components, including L-WT or L-TurboID followed by biotin labeling. Transfected cells were lysed,
153 and biotinylated proteins were captured with streptavidin (SA) beads. Proteins enriched by SA
154 beads were washed and subjected to on-bead trypsin digestion. Digested peptides in solution were
155 labeled with unique tandem-mass tags (TMTs) for quantitative proteomic analysis (**Figure 2A**).
156 To assess the efficiency of the enrichment, biotinylated material bound to SA beads (SA-pull
157 down) from equal amounts of starting material (Input) was eluted in SDS loading buffer containing
158 DTT and biotin and analyzed by western blot. We observed enrichment of biotinylated proteins
159 specific to samples with LAV L-TurboID expression. We observed that only a small fraction of
160 LASV NP was biotinylated, which may reflect that only a low percentage of the total NP participates
161 in the formation of a functional vRNP, or that in the vRNP, the majority of NP was not accessible to
162 biotinylation or remained insoluble under the lysis conditions we used to prepare the proteomic
163 samples. LASV L-TurboID fusion polymerase was also detected in the SA-pull down fraction,
164 suggesting self-biotinylation (**Figure 2B**).
165 To analyze the LASV polymerase interactome, host proteins identified as LASV polymerase
166 interactors were filtered by two criteria: degree of enrichment compared to the control proteome,
167 and the corresponding statistical confidence. The control for the LASV L-TurboID (TurboID_pol)
168 interactome was the interactome of LASV L-WT (WT_pol). For every identified protein, the
169 abundance ratio in the TurboID_pol sample was normalized to that in the WT_pol sample, resulting
170 in the value of fold change. Multiple comparisons were performed across three biological replicates
171 and adjusted *p*-values (adjusted to False Discovery Rate of 0.05) were determined to identify
172 proteins that were enriched in the L-TurboID interactome. A threshold of adjusted *p-value* < 0.05
173 and $\log_2$(fold change) > 1 was used to narrow down high-confidence hits. In summary, we found
174 42 high-confidence hits for cellular proteins that interact with the LASV polymerase (**Figure 2C**).

175 **Effect of siRNA targeting high-confidence LASV polymerase interactors on viral**
176 **infection.** Next, we assessed the importance of LASV polymerase-interacting protein candidates
177 identified by proximity proteomics in authentic LASV infection. For this experiment, we used an
178 siRNA-based functional screen based on well-established experimental procedures (10). Briefly,
179 human hepatocyte Huh7 cells were first transfected with a library of individual siRNAs targeting
180 each of the 42 high-confidence hits, and subsequently infected with the recombinant-LASV-eGFP
181 48 hours post-transfection (11) (**Figure 3A**). siRNA knockdown (KD) of proviral and antiviral
182 candidate host proteins should lead to reduced and enhanced viral infection, respectively. Protein
183 targets with at least two independent siRNA KD resulting in the same infection phenotype across
184 two experiments were considered as true hits.
185 Surprisingly, most high-confidence viral polymerase interactors exhibited an antiviral role, as
186 their siRNA-mediated knockdowns increased normalized %LASV-eGFP infection (**Figure 3B and**
187 **S2**). Limited (10 - 20% of cells) infection of non-silencing control (NSC) siRNA transfected cells

188 (**Figure S3**) may have facilitated favoring the detection of enhancement over reduction in infection.
189 Nevertheless, our results were supported by stringent statistical metrics (two independent
190 experiments with two multiplicities of infection (MOIs), four independent siRNAs per target) and
191 guided by quantitative parameters of the resulting phenotype (Relative % infection and cell count).
192 Potential antiviral factors identified for LASV include EIF3CL, EIF4G2, TAGLN2, TUBA1B, and
193 UPF1. Potential proviral factors for LASV include GSPT1, RPL23, and PLK1 (**Figure 3C**).
194 Knockdown of GSPT1 reduces LASV infection, without affecting the cell count. However,
195 knockdown of the latter two, RPL23 and PLK1 reduces cell count as well as LASV infection,
196 complicating definitive interpretation of a proviral effect. It is possible that these host factors support
197 both LASV replication and cell survival during LASV infection.
198 Based on the results of the siRNA screen, we highlighted functional hits in our identified LASV
199 polymerase interactome network. We clustered hits based on their STRING-classified (12) cellular
200 pathways in order to extrapolate distinct cellular pathways relevant to LASV infection (**Figure 4A**).

201 **Role of GSPT1 in LASV gene expression.** To further validate the biological relevance of the
202 interactome results, we focused on the translation termination factor eRF3a/GSPT1 (13), which
203 has not been previously reported to play any specific role in viral infection.
204 First, we used co-immunoprecipitation (co-IP) assays to confirm that GSPT1, identified here by
205 proximity proteomics, physically interacts with LASV L protein. To perform the co-IP experiment,
206 we co-transfected HEK 293T cells with plasmids expressing an N-terminal Flag-tagged GSPT1
207 (long isoform, 68.7 KDa) and LASV L-HA, respectively, in the presence or absence of other viral
208 factors. We found that LASV L-HA consistently immunoprecipitated Flag-GSPT1 in the presence
209 or absence of LASV NP, or LASV NP and LASV minigenome (**Figure 5A**). We next examined the
210 functional consequence of GSPT1 association with both viral polymerases by viral minigenome
211 assays, which measure a combined effect on viral replication, secondary transcription, and the
212 translation of a minigenome reporter. Consistent with results from the siRNA functional screens,
213 we found that depletion of GSPT1 by one experimentally validated siRNA, GSPT1si8, (**Figure S4**)
214 in HEK 293T cells significantly suppresses LASV minigenome activity (**Figure 5B**). In comparison,
215 depletion of GSPT1 did not affect expression of a control eGFP reporter driven by an RNA
216 polymerase II-based expression plasmid.
217 We also examined whether endogenous GSPT1 interacts with LASV polymerase in a cellular
218 context that recapitulates viral RNA synthesis. In HEK 293T control cells, we observed that
219 endogenous GSPT1 exhibited a diffuse nucleocytoplasmic distribution (**Figure 5C**). However, in
220 HEK 293T cells that successfully reconstituted a functional LASV vRNP, as determined by ZsGreen
221 reporter signal, we detected a fraction of cytoplasmic GSPT1 that clustered with the signal of LASV
222 L-HA (**Figure 5D**), suggesting that GSPT1 can interact with LASV L inside cellular environment.

223 **Role of GSPT1 in LASV multiplication.** To validate the role of GSPT1 on LASV multiplication, we
224 examined the phenotype of GSPT1 knock-down (KD) in multi-step LASV growth kinetics in Huh7
225 cells. Consistent with the results of the siRNA screen, GSPT1 depletion significantly impaired LASV
226 growth in Huh7 cells with at least one log reduction of viral titer 48 hours post-infection (h.p.i.)
227 (**Figure 6A**, 48 h.p.i.). This result supports the proviral role of GSPT1 in LASV infection. Given the
228 known engagement of GSPT1 in cellular nonsense-mediated mRNA decay (NMD) (14, 15), we
229 wondered whether the reduced viral titer was an outcome of decreased LASV mRNA accumulation
230 in infected cells. However, the levels of accumulated LASV vRNA and c/mRNA (s-segment) at 6
231 h.p.i. were all unchanged in GSPT1-depleted cells (**Figure 6B**). In contrast, we observed that LASV
232 GP2 protein levels were diminished in GPST1-depleted cells at 72 h.p.i. (**Figure 6C**). This finding
233 may reflect the role of GSPT1 as a translation termination factor that mediates nascent peptide-
234 chain release and ribosome recycling. Given unchanged LASV mRNA and decreased LASV GP2
235 protein levels, we reason that GSPT1 supports LASV infection perhaps by assisting viral protein
236 translation.
237 Based on the effect of GSPT1 knockdown in LASV growth kinetics, we predicted that
238 pharmacological inhibition of GSPT1 would suppress LASV multiplication. We therefore tested the
239 antiviral activity of CC-90009, a cereblon E3 ubiquitin ligase modulator, which selectively targets

GSPT1 for proteasomal degradation (16, 17) (**Figure 6D**). We treated Huh7 cells with CC-90009 immediately following LASV infection and measured the impact of CC-90009 treatment on the LASV growth curve, viral RNAs, and protein accumulation. At 0.1 and 1 μM, CC-90009 effectively inhibited LASV growth (**Figure 6E**), which correlated with the dose-dependent reduction of both vRNA and c/mRNAs accumulation within 6 hours of viral infection (**Figure 6F**) and diminished viral protein accumulation compared to the DMSO-treated control (**Figure 6G**), without exhibiting cytotoxicity (**Figure 6H**). Together, these results demonstrate that CC-90009 has potent antiviral activity against LASV in human hepatocytes by targeting GSPT1.

Discussion

Here we have presented the first host interactome of LASV polymerase in the context of viral RNA synthesis directed by an intracellular reconstituted vRNP. We first applied proximity-labeling technologies to identify the LASV polymerase interactors *in situ*. We then performed an siRNA screen in human hepatocytes infected with LASV to identify polymerase interactors functionally important during LASV infection. Our finding that most identified polymerase-interactors exhibited an antiviral rather than proviral phenotype could reflect that the viral polymerase itself or the RNA products that it synthesizes are targets of host innate defense mechanisms. Nevertheless, we validated one proviral factor, GSPT1, and demonstrated that it is a druggable target for abrogating LASV infection in cell cultures.

We identified 42 high-confidence LASV polymerase interacting cellular proteins. Among these high-confidence hits, 11 have been previously reported to interact with the NP and L protein of lymphocytic choriomeningitis virus (LCMV), an Old World mammarenavirus related to LASV, via affinity purification-mass spectrometry (AP-MS) approaches in the context of viral infection (18, 19). LCMV is a Biosafety level-2 (BSL2) infectious agent. In contrast, live LASV infection requires the use of BSL4 containment, which complicates proteomic experiments with LASV-infected cells. To overcome this obstacle, we used the TurboID-based, proximity-labeling approach to capture both stable and dynamic protein-protein interactions in the context of a cell-based MG system that recapitulates the biological activities of the LASV vRNP activity. The overlap between the LASV L proximity interactome described here and previously reported LCMV L and NP interactomes (**Figure 4B**) likely reflects conserved molecular recognition interfaces between host cells and Old World mammarenaviruses. Our siRNA-based functional validation studies of the LASV L interactome identified only six, among a total of 42, hits of which depletion significantly impacted LASV infection. This may reflect the limited dynamic range of the siRNA screen in LASV-infected Huh7 cells, despite the stringent thresholds we used to determine all significant functional interactors.

Many RNA viruses have evolved strategies to manipulate the host translational machinery to favor translation initiation of viral mRNAs (20-22). We identified two translation initiation factors in our LASV polymerase interactome, EIF4G2 and EIF3CL, as repressors of LASV infection. EIF4G2 is a functional homolog of EIF4G1 (23), which is known to bridge the high-affinity cytoplasmic cap-binding protein EIF4E, which binds to cap-containing mRNAs, and a scaffolding protein EIF3, which in turn binds to the small ribosomal subunit. In addition, EIF4G2 can enhance the interaction between EIF4E and cap-containing mRNAs (24). As with other mammarenaviruses, transcription of LASV mRNAs uses a 'cap-snatching' mechanism by which viral mRNAs hijack their 5' cap structures from host mRNA species (25), which primes the viral transcription and enables cap-dependent translation mediated by host ribosome (26). Although still controversial, the process whereby mammarenaviruses accomplish "cap-snatching" has been proposed to involve the ability of the virus NP to bind m7GpppN cap structures (27, 28), together with the activity of an endonuclease motif present within the N-terminal region of the LASV polymerase (29) that cleaves cellular mRNAs for acquiring the 5' cap structure. Importantly, the presence of EIF4G2 and EIF3CL but absence of EIF4E in our LASV L interactome suggest that LASV polymerase may not hijack the canonical host cap-binding complex. Instead, based on our results we speculate that L polymerase may compete with the canonical host cap-binding complex (containing EIF4E) for 5' capped cellular mRNAs, and L may bind to EIF4G2 as a decoy that would interfere with stable complex formation between eIF4E and capped mRNAs. This, in turn, would release capped

293 mRNAs to serve as primers for LASV transcription. Additional support for this model stems from
294 the observation that cap-binding affinity of EIF4E was reduced upon binding of LASV Z protein to
295 EIF4E (30), further lowering the affinity barrier for a LASV encoded cap-binding protein, or another
296 proviral factor, to capture fragments of capped cellular mRNAs for priming LASV transcription
297 (**Figure S5**).
298 In addition, our siRNA-based functional screen revealed another LASV polymerase interactor,
299 UPF1, as an antiviral factor. The ATP-dependent RNA helicase upstream frameshift 1 (UPF1) is a
300 key player in multiple cellular RNA decay pathways, typically through binding to the 3' UTR of a
301 target transcript (31), suggesting that UPF1 might play an antiviral role in LASV infection by
302 mediating LASV mRNA decay. We speculate that LASV mRNAs can trigger UPF1-dependent
303 mRNA decay through either the nonsense-mediated mRNA decay (NMD) pathway or another
304 mechanism resembling the replication-dependent histone mRNA decay pathway (HMD) (**Figure**
305 **S6**). In the cellular NMD pathway, UPF1 degrades aberrant RNA transcripts by joining the
306 translation-termination complex (GSPT1/eRF3-eRF1) upon ribosomal recognition of a premature
307 termination codon (PTC) on the mRNA (32). After recruitment to the termination complex, UPF1
308 is phosphorylated, thereby triggering a downstream cascade of nucleases and de-capping
309 enzymes to dismantle the target transcript (33). LASV mRNAs are likely to incorporate premature
310 termination codons owing to the presence of an upstream open reading frame (uORF), which can
311 be acquired by viral transcripts as byproducts of the cap-snatching mechanism (34). In the HMD
312 pathway, phosphorylation of UPF1 is associated with the recognition of 3' UTR stem-loop structure
313 on histone mRNA by the step-loop-binding protein (SLBP). Similar to histone mRNAs, which lack
314 3' poly(A) tail, LASV mRNAs are also non-poly-adenylated and harbor a stem-loop structure on
315 the 3' end (35, 36) due to the LASV intergenic region (IGR) mediated, structure-dependent
316 transcription termination (37, 38). Future experiments are needed to determine whether UPF1-
317 LASV L interaction is RNA-dependent, and whether UPF1 directly targets LASV mRNAs for
318 degradation, perhaps by detecting UPF1 phosphorylation upon intracellular exposure to LASV
319 mRNAs. SLBP was not captured in the LASV polymerase interactome, but we cannot rule out the
320 possibility that SLBP recognizes the 3' stem-loop on LASV mRNAs. These findings provide the first
321 evidence of a possible participation of the host RNA quality control mechanisms on modulating
322 mammarenavirus infection.
323 We also identified DIS3 and PUM1 as LASV polymerase interactors. DIS3 is the catalytic subunit
324 of host exosome complex, which participates in the downstream RNA degradation of UPF1-
325 dependent mRNA decays (31), and contains both 3'-to-5' exoribonuclease and endoribonuclease
326 activities (39). PUM1 is a sequence-dependent RNA sensor protein, which targets specific mRNAs
327 for post-transcriptional degradation (40, 41). Since none of the LASV 3' UTRs contains the PUM1
328 consensus sequence (5'-UGUAHAUA-3'), it is unlikely that PUM1 targets LASV mRNAs for
329 degradation. We speculate that LASV polymerase may selectively hijack key components of
330 cellular mRNA decay pathway to harvest 5'-capped fragments of cellular transcripts. In this context,
331 a subset of cellular mRNAs targeted by PUM1 and undergoing PUM1-mediated mRNA
332 destabilization can be retrieved by LASV polymerase for the 5' cap structure before RNases such
333 as DIS3 reach the 5' end of dismantled transcripts (**Figure S7**). The identification of multiple cellular
334 mRNA decay components as LASV L interactors opens new directions on the investigation of the
335 molecular basis of LASV cap-snatching.
336 G1-to-S-phase transition 1(GSPT1)/eukaryotic peptide chain release factor GTP-binding
337 subunit A(eRF3a) was the only L-interactor that exhibited a proviral phenotype. GSPT1 is a core
338 component of the cellular translation termination machinery (13, 42), also participates in the cellular
339 NMD pathway, and has been shown to regulate cell cycle progression (43) and promote apoptosis
340 (44). As GSPT1 participates in multiple cellular pathways, it may regulate viral infection via different
341 mechanisms in a context-dependent manner. Results from co-IP assays showed a physical
342 association between LASV L polymerase and GSPT1, supporting the validity of proximity labeling-
343 based proteomics to identify *bona fide* LASV L-interactors. GSPT1 knock-down resulted in
344 significantly reduced production of LASV infectious progeny in a multi-step growth kinetics
345 experiment. This result correlates with a role of GSPT1 supporting viral protein translation, without

346 significantly affecting the accumulation of viral RNA species. Whether the proviral phenotype we
347 have observed in GSPT1 is indirectly mediated by its involvement in regulating cell cycle or
348 apoptosis remains to be determined. Future studies are needed to assess the functional
349 consequence of the physical association between GSPT1 and LASV polymerase and to verify
350 whether GSPT1 contributes to any step of LASV RNA synthesis. Notably, we found that CC-90009,
351 a cereblon E3 ligase modulating drug which specifically targets GSPT1 for proteasomal
352 degradation, exhibited potent antiviral activity against LASV without appreciable cytotoxicity. The
353 fact that CC-90009 is currently in phase 1 clinical development for the treatment of acute myeloid
354 leukemia (AML) raises the interesting possibility of exploring its repurposing as an antiviral drug
355 against LASV.
356 In summary, we have presented here the first comprehensive proximity interactome of the LASV
357 polymerase in the context of viral replication. For the proximity proteomics experiment, we used a
358 cell-based LASV MG system that recreates the molecular events associated with viral RNA
359 synthesis during *bona fide* LASV infection. We validated the protein-protein interaction networks
360 using an siRNA-based, functional screen with authentic LASV infection. As a proof-of-concept, we
361 characterized the mechanisms of action by which GSPT1, a novel host factor identified here for the
362 first time as a proviral factor required for LASV infection. Further work is required to explore the
363 role of these functional interactors in other primary target cells including macrophage and dendritic
364 cells and in suitable animal models. Likewise, the antiviral effect of CC-90009, a pharmacological
365 compound targeting GSPT1, should be examined in other related arenaviruses. Together, our
366 findings illuminate new mechanisms of host regulation of LASV replication and reveal a landscape
367 of novel targets for host-directed antiviral drug development.

368 **Materials and Methods**

369 **Plasmids, siRNAs, antibodies, primers:** see SI Appendix.

370 **Cell cultures and viruses:** see SI Appendix.

371 **Compound:** CC-90009 (GSPT1-targeting compound) was purchased from MedKoo Biosciences
372 (Cat# 207005).

373 **LASV minigenome (MG) assay:** HEK 293T cells (2×10^5 per well) were seeded in 24-well plates
374 one day prior to transfection with the following plasmids: 300 ng pCAGGS-T7 polymerase, 300 ng
375 pCAGGS-LASV MG encoding a ZsGreen fluorescent reporter, 300 ng pCAGGS-LASV-L, 150 ng
376 pCAGGS-LASV-NP. In some cases: pCAGGS-LASV-L was replaced with a tagged variant. A
377 control was included in every assay in which the pCAGGS-L plasmid was omitted to verify active
378 MG RNA synthesis mediated by LASV L. Plasmids were transfected with Lipofectamine 3000
379 transfection reagent (1.5 µl/well). At 72 hours post-transfection, cell lysates were collected and
380 measured for green fluorescence intensity.

381 **Biotinylation with polymerase-TurboID fusion protein:** See *SI Appendix* for experimental
382 details.

383 **Immunofluorescent analysis (IFA) using confocal microscopy:** Acetone cleaned, glass
384 coverslips (1.5 mm thickness) placed inside 24-wells were treated with human fibronectin (50
385 mg/ml) for 20 min at 37 ℃ incubator, prior to HEK 293T cells seeding ($4X10^4$/well). Twenty-four
386 hours later, the monolayer was transfected with the LASV minigenome system using Trans-IT LT1
387 as described. For in-cell biotinylation experiment, biotin (500 µM final concentration) was added to
388 the culture media allowing for one hour in-cell biotinylation of cells transfected with the LASV MG
389 components. Labeling was stopped by washing cells with cold DPBS. For all IFA specimens, cells
390 were fixed in 4% paraformaldehyde for 15 mins at room temperature, permeabilized with 0.1%
391 Triton-X100 for 10 mins, and blocked in 1% normal goat serum for at least one hour. Primary
392 antibody incubations were performed at room temperature for two hours or at 4 ℃ overnight.

393 Specimens were washed three times with PBS-0.1% Tween-20 and incubated with secondary
394 antibodies for one hour at room temperature. Nuclei were counterstained by Hoechst. Confocal
395 images were acquired on Zeiss LSM880-airyscan system under super-resolution mode, using a
396 63x/NA1.4 oil objective. Please see *SI Appendix* for full description of antibodies used in IFA
397 experiments.

398 **Proximity labeling-based proteomics (sample preparation, quality control, proteomic**
399 **experiment, and data analysis):** See *SI Appendix* for details.

400 **siRNA functional screening:** Huh7 cells (5 x 10^3 per well) were seeded in clear-bottom, black 96-
401 wells plate, leaving edge wells filled with DPBS. Twenty-four hours, Huh7 monolayers were
402 transfected with 10 nM of individual siRNAs using Lipofectamine RNAiMAX (0.1 ul per well). Knock
403 down (KD) of each target was performed using four individual siRNA transfections, each one
404 performed in triplicate. Each plate includes two sets of triplicated internal control wells transfected
405 with 10 nM All Star negative control (NSC) to account for plate-to-plate variations. Forty-eight hours
406 later, plates were transferred to BSL4 for infection with LASV-eGFP at indicated MOIs. Infected
407 monolayers were fixed and inactivated by 10% formalin at two days post infection and removed
408 from BSL4 facility. Percentage of LASV-eGFP infected Huh7 cells (% infection) with different siRNA
409 treatment were quantified by high-content imager CX5 using a 10x objective. Cell count in each
410 well was determined by the number of Hoechst-stained nuclei. Data analysis of siRNA screen
411 described in *SI Appendix*.

412 **Viral growth kinetics and quantification of viral proteins and RNAs:** Huh7 cells (5 × 10^4 per
413 well) were seeded in 24-well plates and transfected with 10 nM siRNA (NSC or GSPT1 si8,
414 experimentally validated) the next day as described above or incubated with 0.1 μM GSPT1
415 inhibitor (CC-90009) or DMSO. Forty-eight hours after transfection, Huh7 monolayers were
416 transferred into BSL-4 facilities and infected with LASV-eGFP at MOI of 0.5 (PFU/ml) for one hour.
417 Infection of the cells was followed by removal of the inoculum and replenishing with 2% FBS
418 containing fresh media. For virus titration, aliquots of supernatant were harvested at indicated time
419 points from infected monolayers and used to infect Vero-E6 cells for foci-quantification. At indicated
420 time points, infected Huh7 monolayers were collected directly in Trizol or 4x Laemmli buffer for
421 inactivation and downstream RNA/protein quantifications. Equal volume of Laemmli lysates were
422 loaded on SDS-PAGE gel for western blot analysis. Equal amount of total RNA in each sample was
423 used for strand-specific RT-qPCR.

424 **Co-immunoprecipitation:** Full description in *SI Appendix*.

425 **Cell viability quantification by Cell-titer Glo assay:** Full description in *SI Appendix*.

426 **Acknowledgments**
427
428 We thank Beatrice Cubitt from de la Torre Lab (Scripps Research, CA) for helping with the cloning
429 of pCI-FLAG-GSPT1 plasmid and preparing LASV minigenome plasmid stocks. Special thanks to
430 Catherine Shuang Liu (Scripps Research, CA) for helping with ChemDraw. We thank Zbigniew
431 Mikulski of the Microscopy Core Facility at La Jolla Institute for Immunology for assistance, and
432 NIH S10OD021831 for sponsoring the Zeiss LSM 880 microscope. This research was supported
433 by institutional funds of La Jolla Institute for Immunology. J.F. was supported by the Donald E. and
434 Delia B. Baxter Foundation Fellowship. This is the publication # 30107 from Scripps Research.
435
436

437
438 **References**

439 1. Asogun DA, Gunther S, Akpede GO, Ihekweazu C, & Zumla A (2019) Lassa Fever:
440 Epidemiology, Clinical Features, Diagnosis, Management and Prevention. *Infect Dis Clin*
441 *North Am* 33(4):933-951.
442 2. Kofman A, Choi MJ, & Rollin PE (2019) Lassa Fever in Travelers from West Africa, 1969-
443 2016. *Emerg Infect Dis* 25(2):245-248.
444 3. Rojek JM & Kunz S (2008) Cell entry by human pathogenic arenaviruses. *Cell Microbiol*
445 10(4):828-835.
446 4. Ortin J & Martin-Benito J (2015) The RNA synthesis machinery of negative-stranded RNA
447 viruses. *Virology* 479-480:532-544.
448 5. Morin B, Kranzusch PJ, Rahmeh AA, & Whelan SP (2013) The polymerase of negative-
449 stranded RNA viruses. *Curr Opin Virol* 3(2):103-110.
450 6. Peng R*, et al.* (2020) Structural insight into arenavirus replication machinery. *Nature*
451 579(7800):615-619.
452 7. Branon TC*, et al.* (2018) Efficient proximity labeling in living cells and organisms with
453 TurboID. *Nat Biotechnol* 36(9):880-887.
454 8. Vogel D, Rosenthal M, Gogrefe N, Reindl S, & Gunther S (2019) Biochemical
455 characterization of the Lassa virus L protein. *J Biol Chem* 294(20):8088-8100.
456 9. Martinez-Sobrido L, Paessler S, & de la Torre JC (2017) Lassa Virus Reverse Genetics.
457 *Methods Mol Biol* 1602:185-204.
458 10. Fang J*, et al.* (2018) Staufen1 Interacts with Multiple Components of the Ebola Virus
459 Ribonucleoprotein and Enhances Viral RNA Synthesis. *mBio* 9(5).
460 11. Cai Y*, et al.* (2018) Recombinant Lassa Virus Expressing Green Fluorescent Protein as a
461 Tool for High-Throughput Drug Screens and Neutralizing Antibody Assays. *Viruses*
462 10(11).
463 12. Szklarczyk D*, et al.* (2019) STRING v11: protein-protein association networks with
464 increased coverage, supporting functional discovery in genome-wide experimental
465 datasets. *Nucleic Acids Res* 47(D1):D607-D613.
466 13. Zhouravleva G*, et al.* (1995) Termination of translation in eukaryotes is governed by two
467 interacting polypeptide chain release factors, eRF1 and eRF3. *EMBO J* 14(16):4065-4072.
468 14. Aliouat A*, et al.* (2020) Divergent effects of translation termination factor eRF3A and
469 nonsense-mediated mRNA decay factor UPF1 on the expression of uORF carrying
470 mRNAs and ribosome protein genes. *RNA Biol* 17(2):227-239.
471 15. Hoshino S (2012) Mechanism of the initiation of mRNA decay: role of eRF3 family G
472 proteins. *Wiley Interdiscip Rev RNA* 3(6):743-757.
473 16. Hansen JD*, et al.* (2021) CC-90009: A Cereblon E3 Ligase Modulating Drug That Promotes
474 Selective Degradation of GSPT1 for the Treatment of Acute Myeloid Leukemia. *J Med*
475 *Chem* 64(4):1835-1843.
476 17. Baradaran-Heravi A*, et al.* (2021) Effect of small molecule eRF3 degraders on premature
477 termination codon readthrough. *Nucleic Acids Res* 49(7):3692-3708.
478 18. Khamina K*, et al.* (2017) Characterization of host proteins interacting with the
479 lymphocytic choriomeningitis virus L protein. *PLoS Pathog* 13(12):e1006758.
480 19. Iwasaki M*, et al.* (2018) Interactome analysis of the lymphocytic choriomeningitis virus
481 nucleoprotein in infected cells reveals ATPase Na+/K+ transporting subunit Alpha 1 and

482 prohibitin as host-cell factors involved in the life cycle of mammarenaviruses. *PLoS*
483 *Pathog* 14(2):e1006892.
484 20. Leen EN*, et al.* (2016) A Conserved Interaction between a C-Terminal Motif in Norovirus
485 VPg and the HEAT-1 Domain of eIF4G Is Essential for Translation Initiation. *PLoS Pathog*
486 12(1):e1005379.
487 21. Burgui I, Yanguez E, Sonenberg N, & Nieto A (2007) Influenza virus mRNA translation
488 revisited: is the eIF4E cap-binding factor required for viral mRNA translation? *J Virol*
489 81(22):12427-12438.
490 22. Connor JH & Lyles DS (2002) Vesicular stomatitis virus infection alters the eIF4F
491 translation initiation complex and causes dephosphorylation of the eIF4E binding
492 protein 4E-BP1. *J Virol* 76(20):10177-10187.
493 23. Gradi A*, et al.* (1998) A novel functional human eukaryotic translation initiation factor
494 4G. *Mol Cell Biol* 18(1):334-342.
495 24. Gross JD*, et al.* (2003) Ribosome loading onto the mRNA cap is driven by conformational
496 coupling between eIF4G and eIF4E. *Cell* 115(6):739-750.
497 25. Lelke M, Brunotte L, Busch C, & Gunther S (2010) An N-terminal region of Lassa virus L
498 protein plays a critical role in transcription but not replication of the virus genome. *J*
499 *Virol* 84(4):1934-1944.
500 26. Olschewski S, Cusack S, & Rosenthal M (2020) The Cap-Snatching Mechanism of
501 Bunyaviruses. *Trends Microbiol* 28(4):293-303.
502 27. Brunotte L*, et al.* (2011) Structure of the Lassa virus nucleoprotein revealed by X-ray
503 crystallography, small-angle X-ray scattering, and electron microscopy. *J Biol Chem*
504 286(44):38748-38756.
505 28. Qi X*, et al.* (2010) Cap binding and immune evasion revealed by Lassa nucleoprotein
506 structure. *Nature* 468(7325):779-783.
507 29. Reguera J*, et al.* (2016) Comparative Structural and Functional Analysis of Bunyavirus
508 and Arenavirus Cap-Snatching Endonucleases. *PLoS Pathog* 12(6):e1005636.
509 30. Volpon L, Osborne MJ, Capul AA, de la Torre JC, & Borden KL (2010) Structural
510 characterization of the Z RING-eIF4E complex reveals a distinct mode of control for
511 eIF4E. *Proc Natl Acad Sci U S A* 107(12):5441-5446.
512 31. Kim YK & Maquat LE (2019) UPFront and center in RNA decay: UPF1 in nonsense-
513 mediated mRNA decay and beyond. *RNA* 25(4):407-422.
514 32. Kurosaki T & Maquat LE (2016) Nonsense-mediated mRNA decay in humans at a glance.
515 *J Cell Sci* 129(3):461-467.
516 33. Kurosaki T, Popp MW, & Maquat LE (2019) Quality and quantity control of gene
517 expression by nonsense-mediated mRNA decay. *Nat Rev Mol Cell Biol* 20(7):406-420.
518 34. Ho JSY*, et al.* (2020) Hybrid Gene Origination Creates Human-Virus Chimeric Proteins
519 during Infection. *Cell* 181(7):1502-1517 e1523.
520 35. Meyer BJ & Southern PJ (1993) Concurrent sequence analysis of 5' and 3' RNA termini by
521 intramolecular circularization reveals 5' nontemplated bases and 3' terminal
522 heterogeneity for lymphocytic choriomeningitis virus mRNAs. *J Virol* 67(5):2621-2627.
523 36. Scheslenok EP, Stel'makh TA, Shkolina TV, & Lukashevich IS (1988) [Template activity of
524 poly(A+) and poly(A-) messenger RNA of pathogenic arenaviruses]. *Mol Gen Mikrobiol*
525 *Virusol* (7):29-31.

526 37. Lopez N & Franze-Fernandez MT (2007) A single stem-loop structure in Tacaribe
527 arenavirus intergenic region is essential for transcription termination but is not required
528 for a correct initiation of transcription and replication. *Virus Res* 124(1-2):237-244.
529 38. Pinschewer DD, Perez M, & de la Torre JC (2005) Dual role of the lymphocytic
530 choriomeningitis virus intergenic region in transcription termination and virus
531 propagation. *J Virol* 79(7):4519-4526.
532 39. Schaeffer D*, et al.* (2009) The exosome contains domains with specific
533 endoribonuclease, exoribonuclease and cytoplasmic mRNA decay activities. *Nat Struct*
534 *Mol Biol* 16(1):56-62.
535 40. Goldstrohm AC, Hall TMT, & McKenney KM (2018) Post-transcriptional Regulatory
536 Functions of Mammalian Pumilio Proteins. *Trends Genet* 34(12):972-990.
537 41. Morris AR, Mukherjee N, & Keene JD (2008) Ribonomic analysis of human Pum1 reveals
538 cis-trans conservation across species despite evolution of diverse mRNA target sets. *Mol*
539 *Cell Biol* 28(12):4093-4103.
540 42. Frolova L*, et al.* (1996) Eukaryotic polypeptide chain release factor eRF3 is an eRF1- and
541 ribosome-dependent guanosine triphosphatase. *RNA* 2(4):334-341.
542 43. Chauvin C, Salhi S, & Jean-Jean O (2007) Human eukaryotic release factor 3a depletion
543 causes cell cycle arrest at G1 phase through inhibition of the mTOR pathway. *Mol Cell*
544 *Biol* 27(16):5619-5629.
545 44. Hegde R*, et al.* (2003) The polypeptide chain-releasing factor GSPT1/eRF3 is
546 proteolytically processed into an IAP-binding protein. *J Biol Chem* 278(40):38699-38706.

547

548

549 **Figures and figure legends**

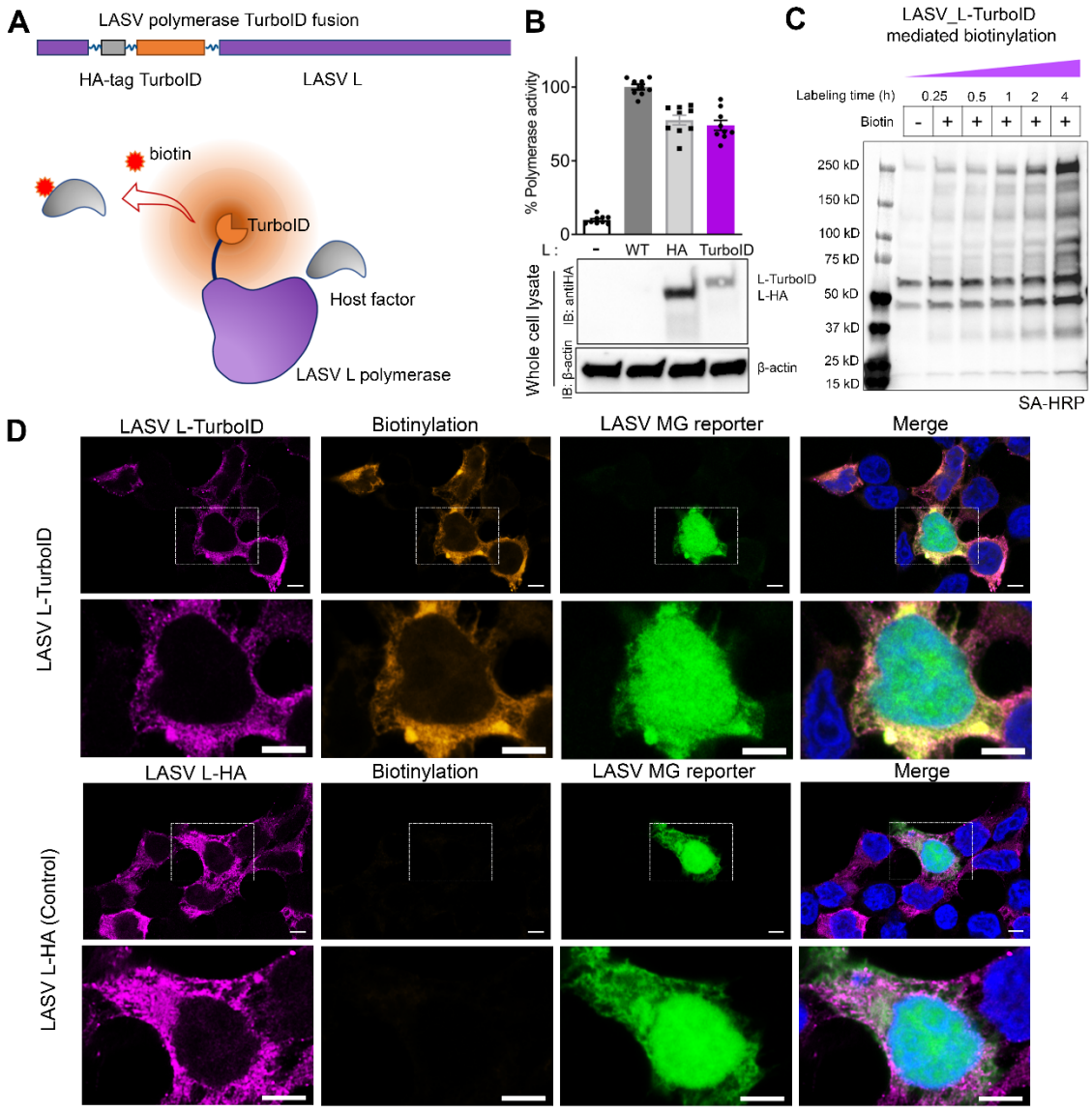

550

551 **Figure 1. Generation of a functional LASV polymerase with proximity-labeling activity.**

552 (A) Expression construct of LASV L-TurboID fusion polymerase and a schematic describing
553 proximity biotinylation of LASV L interacting host factors. (B) Polymerase activity and expression
554 of LASV L-TurboID compared to wild-type L and HA-tagged L in cells transfected with the LASV
555 minigenome (MG) components. ZsGreen fluorescence signal was quantified in each sample and
556 normalized to the L-WT control. Representative western blots showing expression of LASV L
557 variants and β-actin in HEK293T lysates. LASV MG assay was repeated in three independent
558 replicates with triplicated wells for each condition. Bar graphs containing nine individual data points
559 for each condition are displayed, with means plus standard error of the means/SEM (error bars).
560 Two-tailed, unpaired t tests were performed comparing activity of different polymerase variants to
561 the wild-type controls. Values significantly different from the controls are indicated by asterisks as
562 follows: *, $P < 0.05$; **, $P < 0.01$; ***, $P < 0.001$. (C) Streptavidin blot demonstrating biotin ligase
563 activity of LASV L-TurboID in cells transfected with the LASV MG components. (D) Confocal

immunofluorescence images of LASV L-TurboID mediated proximity biotinylation in cells co-expressing the LASV MG components. LASV L-HA and L-TurboID were detected by using an anti-HA antibody. Biotinylated proteins were detected by using the streptavidin-AF594. Scale bar: 5 µm. Representative images acquired by Zeiss-LSM880 Airyscan from two independent experiments are shown. Each experiment includes at least three different fields of view.

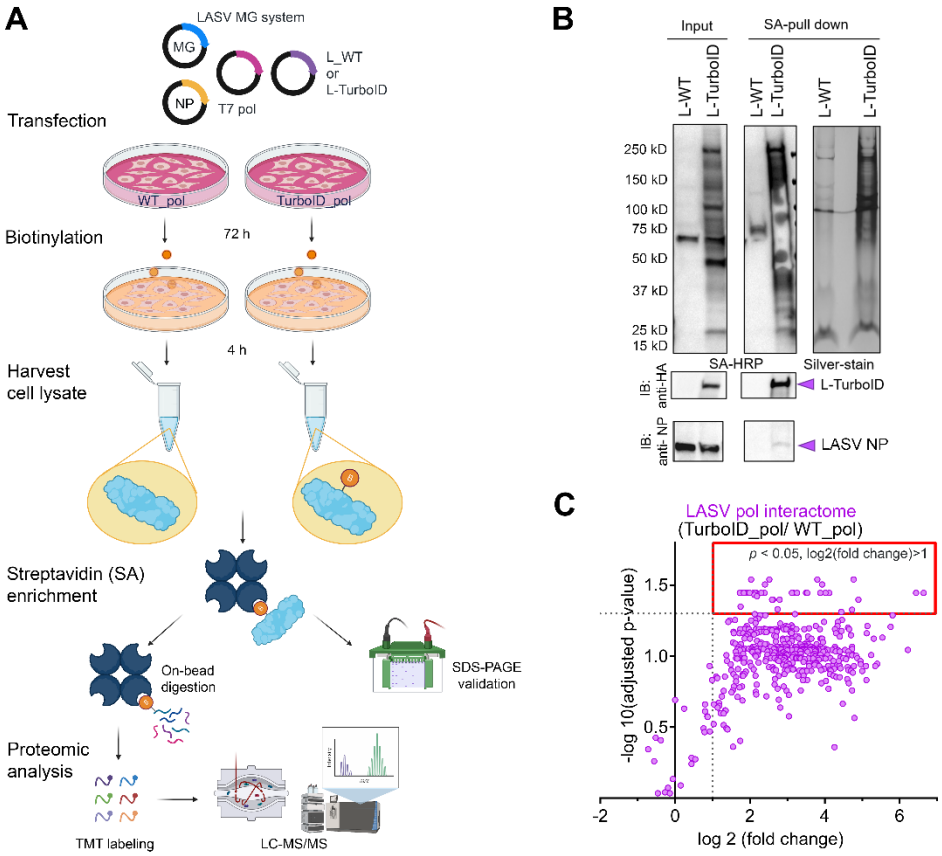

Figure 2. Proximity proteomics of LASV polymerase in living cells.

(A) Proximity proteomic sample preparation workflow. (B) Validation of streptavidin enrichment of LASV L-TurboID mediated proximity biotinylation. Total lysates are indicated as “Input”, biotinylated proteins enriched by streptavidin magnetic beads and indicated as “SA-pull down”. Representative blots and a silver-stained gel of three biological replicates are presented. (C) A scatter plot showing LASV polymerase interacting proteins in HEK 293T cells determined by quantitative proteomic analysis. For each protein, its degree of enrichment indicated by fold change and statistical confidence of enrichment, which is indicated by adjusted p-value, are numerated and log transformed. High-confidence hits are highlighted by red rectangular box.

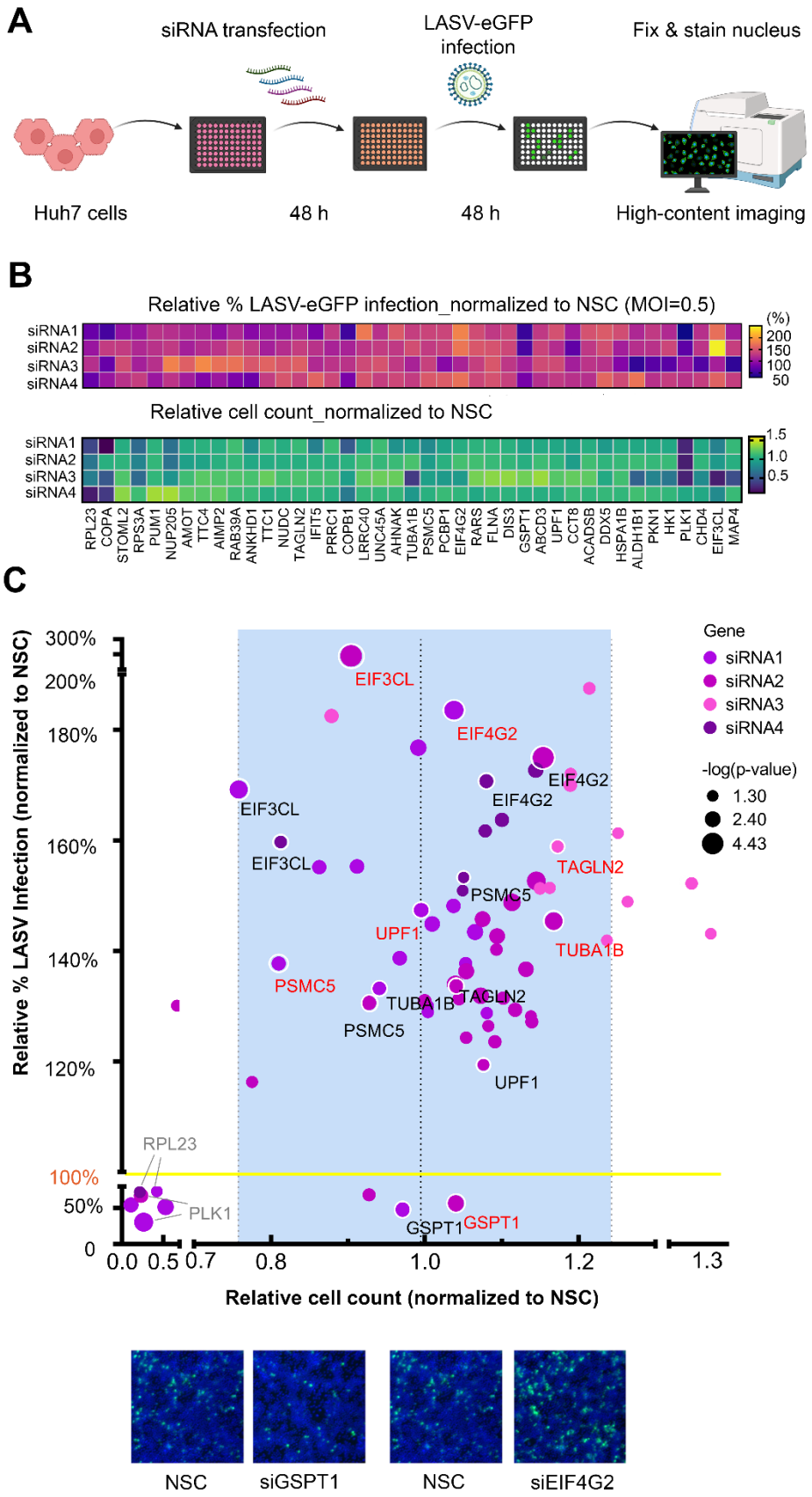
A
siRNA transfection
LASV-eGFP infection
Fix & stain nucleus
Huh7 cells
48 h
48 h
High-content imaging
B
Relative % LASV-eGFP infection_normalized to NSC (MOI=0.5)
siRNA1
siRNA2
siRNA3
siRNA4
(%)
200
150
100
50
Relative cell count_normalized to NSC
1.5
1.0
0.5
RPL23 COPA STOML2 RPS3A PUM1 NUP205 AMOT TTC4 AIMP2 RAB39A ANKHD1 TTC1 NUDC TAGLN2 IFIT5 PRRC1 COPB1 LRRC40 UNC45A AHNAK TUBA1B PSMC5 PCBP1 EIF4G2 RARS FLNA DIS3 GSPT1 ABCD3 UPF1 CCT8 ACADSB DDX5 HSPA1B ALDH1B1 PKN1 HK1 PLK1 CHD4 EIF3CL MAP4
C
Relative % LASV Infection (normalized to NSC)
300%
200%
180%
160%
140%
120%
100%
50%
0
Relative cell count (normalized to NSC)
0.0 0.5 0.7 0.8 1.0 1.2 1.3
Gene
siRNA1
siRNA2
siRNA3
siRNA4
-log(p-value)
1.30
2.40
4.43
EIF3CL
EIF4G2
EIF4G2
EIF4G2
EIF3CL
EIF3CL
TAGLN2
PSMC5
UPF1
TUBA1B
PSMC5
TUBA1B
TAGLN2
PSMC5
UPF1
RPL23
PLK1
GSPT1
GSPT1
NSC
siGSPT1
NSC
siEIF4G2

579

580 **Figure 3. Identification of functional polymerase interactors by siRNA screen in LASV-**
581 **infected cells.** (A) Workflow of siRNA screen by high-content imaging of virus infected Huh7 cells.
582 Raw percentage of infection and cell count of each siRNA treatment were normalized to that of
583 non-silencing controls (NSC), respectively. (B) Normalized values are displayed in heat maps of
584 relative percentage of infection and relative cell count for LASV. Each value is the mean of technical
585 triplicates. Multiple unpaired t tests were performed to determine the statistical significance of
586 siRNA-mediated changes on percentage of infection compared to that of NSC. Determined *p*-
587 values were log-transformed and displayed as the size of each data point on a scatter plot for LASV
588 (C). Data points in the heatmap with a *p*-value > 0.05 were eliminated from the scatter plot. Genes
589 for which multiple siRNAs significantly affected infection are labeled on the corresponding data
590 points; one label is in red for display purpose. Representative fluorescent images of Huh7
591 monolayer at 48 hours post infection are shown with LASV-eGFP infected cells in green and nuclei
592 in blue for NSC and selected siRNA treatment. One representative result from two rounds of siRNA
593 screen using different MOIs is shown.

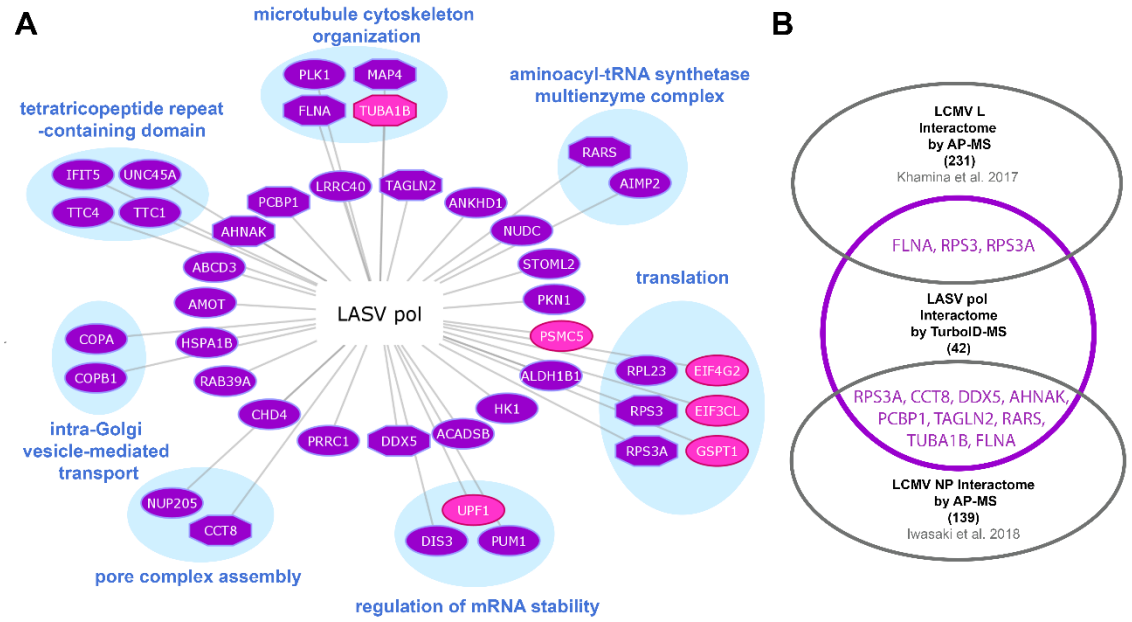

594

595 **Figure 4. The proximity interactome of LASV polymerase.** (A) Network display of the LASV
596 polymerase interactome identified by proximity proteomics. Each node represents one high-
597 confidence proteomic hit. Each edge represents identified protein-protein interaction. Nodes that
598 are functionally validated by siRNA screen are highlighted in pink. Nodes shown in heptagons have
599 been previously reported for other virus-host interactomes. Selected nodes are clustered based on
600 enriched biological processes or protein domains by functional enrichment analyses via STRING.
601 (B) A Venn diagram comparing cellular interactors of LASV polymerase with previously reported
602 interactors of LCMV proteins.

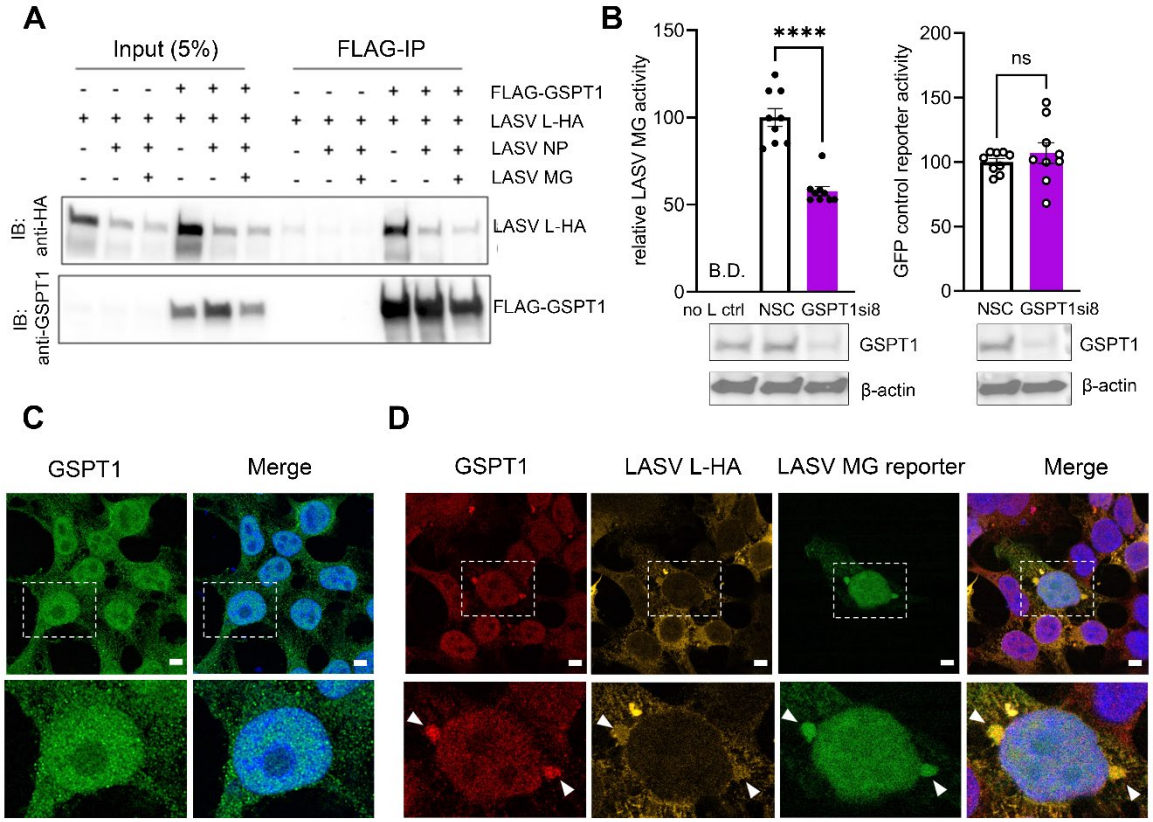

603

604 **Figure 5. GSPT1 physically and functionally associates with LASV polymerase**. (A) Western
605 blot analyses of LASV L-HA co-immunoprecipitated with Flag-GSPT1. Representative result of
606 three biological replicates is shown. (B) LASV MG activity and expression level of a control GFP
607 reporter in GSPT1-depleted HEK 293T cells. GSPT1 depletion by siRNA was validated by western
608 blot analysis. MG activity and expression level of the control GFP reporter in GSPT1si8 transfected
609 cells were normalized to that of NSC. The LASV MG experiment was repeated in three independent
610 replicates with triplicated wells for each condition. Bar graphs containing nine individual data points
611 for each condition are displayed, with means plus SEM (error bars). Two-tailed, unpaired t tests
612 were performed to determine whether depleting or overexpressing GSPT1 significantly changed
613 activities of viral minigenome and the control reporter. Values that are significantly different from
614 the controls are indicated by asterisks as follows: *, $p < 0.05$; **, $p < 0.01$; ***, $p < 0.001$. Confocal
615 immuno-fluorescent analysis of the subcellular localization of endogenous GSPT1 by itself (C) or
616 with transiently expressed LASV L-HA together with the LASV minigenome system in HEK 293T
617 cells (D). Arrowheads in the zoomed region indicate sites where endogenous GSPT1 localize next
618 to viral proteins. Representative images acquired by Zeiss-LSM880 Airyscan from two independent
619 experiments are shown, each experiment includes at least three different fields of view.

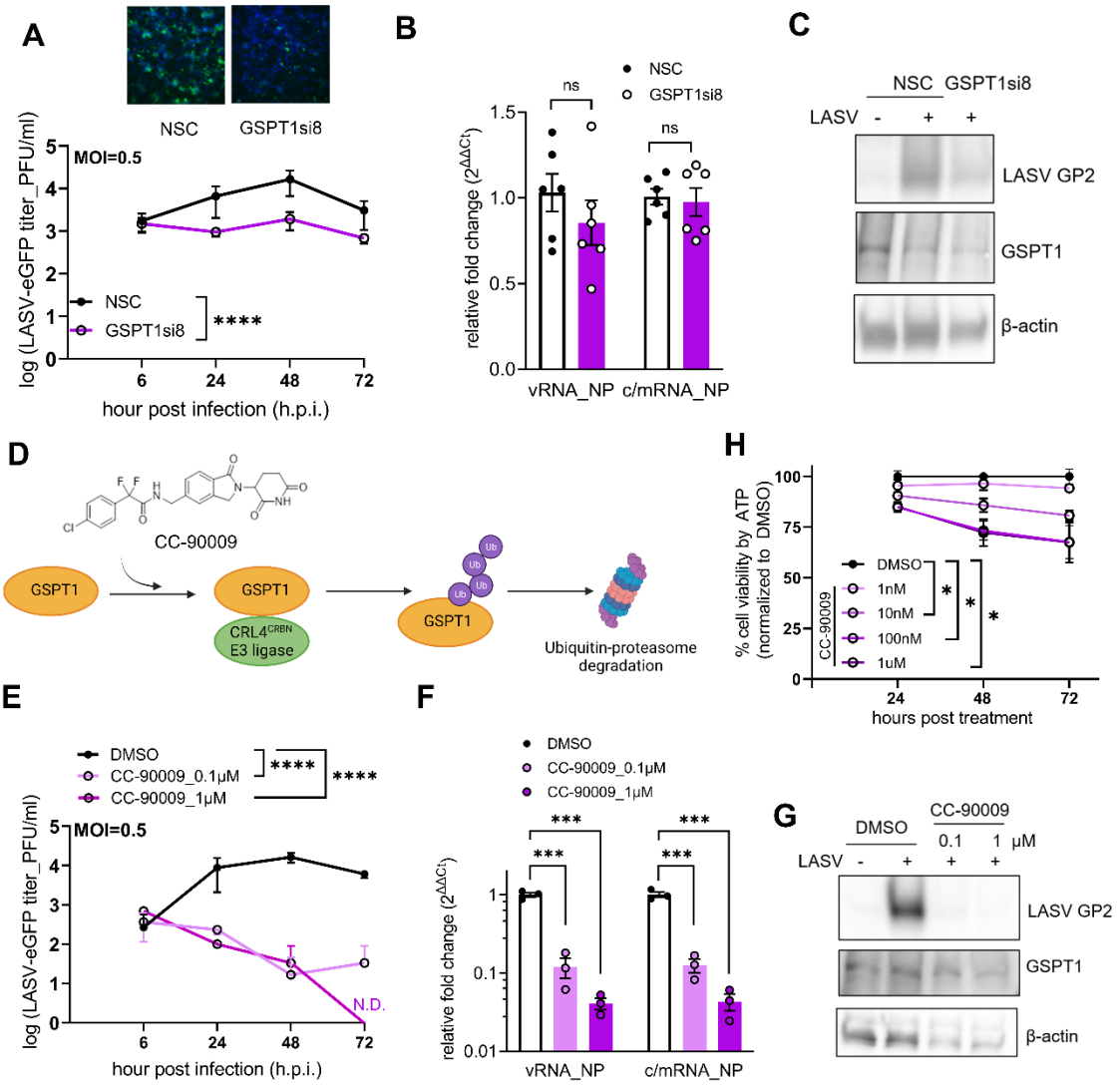

Figure 6. GSPT1 is a druggable host factor required for LASV multiplication. (A) Effect of GSPT1 depletion on LASV viral growth kinetics in Huh7 cells. Representative fluorescent images of Huh7 monolayer at 72 hours post-infection (h.p.i.) are shown with virus infected cells (green) and nuclei (blue). Results of two independent experiments with technical triplicates are plotted as mean and standard deviations (error bars). Two-way ANOVA analysis on log transformed viral titers was performed to determine the statistical significance of the effect of GSPT1 depletion on viral titers. (B) Effect of GSPT1 depletion on LASV vRNA and c/mRNA accumulation at 6 h.p.i.. Six individual data points from two independent experiments with technical triplicates are displayed indicated as mean and SEM (error bars). Values that are significantly different from the controls were determined by two-tailed, unpaired t-test and indicated by asterisks as follows: *, $p < 0.05$; **, $p < 0.01$; ***, $p < 0.001$. (C) Western blot analysis of GSPT1 protein and LASV GP2 levels in lysates from LASV-infected Huh7 cells harvested at 72 h.p.i.. Lysates from triplicate wells in the growth kinetic experiments were pooled and analyzed. Representative blots from one experiment are shown. (D) Schematics of the mode of action for CC-90009 mediated GSPT1-targeted degradation. (E) Effect of CC-90009 on LASV growth kinetics in Huh7 cells. Results of one experiment with technical triplicates are plotted as mean and standard deviations (error bars). N.D: not detectable.

637 Two-way ANOVA analyses on viral titers with Tukey's multiple comparisons were performed to
638 determine the statistical significance of the effect of CC-90009 treatments on LASV titer compared
639 to DMSO treatment. (****, P<0.0001) (F) Effect of CC-90009 treatment on LASV vRNA and c/mRNA
640 accumulation in Huh7 cells at 6 h.p.i.. Six individual data points from two independent experiments
641 with technical triplicates are displayed indicated as mean and SEM (error bars). Values significantly
642 different from the controls were determined by two-tailed, unpaired t-test and indicated by asterisks
643 as follows: *, P < 0.05; **, P < 0.01; ***, P < 0.001. (D) Western blot analysis of GSPT1 protein and
644 LASV GP2 levels in LASV-infected Huh7 lysates harvested at 72 h.p.i.. Lysates from triplicate wells
645 in the growth kinetic experiments were pooled and analyzed. (H) Cell viability of CC-90009 treated
646 Huh7 cells in the absence of viral infection was determined by Cell titer Glo 2.0. Raw values of cell
647 viability in drug treated samples are normalized to DMSO control. Six individual data points from
648 two independent experiments with technical triplicates are combined and indicated as mean and
649 SEM (error bars). Values that are significantly different from the controls are determined by two-
650 way ANOVA and indicated by asterisks as follows: *, P < 0.05.